Supporting Information for "Linking Overturning, Recirculation, and Melt in Glacial Fjords"

Ken X. Zhao[1], Andrew L. Stewart[1], and James C. McWilliams[1]

[1]Department of Atmospheric and Oceanic Sciences, University of California, Los Angeles

Contents of this file

- Text S-1 Model Setup and Plume Parameterizations

- Text S-2 Quasi-Streamfunction Approximation

- Text S-3 Fjord Circulation and Melt Sensitivity to Discharge Plume Strength, Geometry, Stratification, and Tides

- Text S-4 Melt Rate Theory Approximations

- Table S1

- Figures S1 to S8

S-1. Model Setup and Plume Parameterizations

The model used in the study is the Massachusetts Institute of Technology General Circulation Model (MITgcm), which is available at *mitgcm.org*. Using this model, we solve the hydrostatic, Boussinesq primitive equations with a nonlinear equation of state

based on Jackett and McDougall (1995). For the cases with tides (see Table S1), we use a

barotropic tidal velocity (with magnitudes of 0 to 0.1 m/s) with a semi-diurnal frequency.

The plume parameterizations that we implement in the MITgcm model configuration is

a slightly modified version of that proposed by Cowton, Slater, Sole, Goldberg, and Nienow

(2015), optimized to work efficiently in high resolution simulations, and is available at:

https://doi.org/10.5281/zenodo.5214142. This is identical to the parameterization pack-

age detailed in Cowton et al. (2015), except that we redistribute the buoyancy anomalies

from the solutions to the discharge plume equations over a 10-gridpoint radius semi-circle

in the horizontal and apply a 3-gridpoint smoothing in the vertical while conserving the

overall buoyancy anomaly and entrainment. This prevents prohibitive restrictions set by

the Courant-Friedrichs-Lewy (CFL) condition on the model timestep in our high resolu-

tion simulations as well as spurious mixing caused by sharp gradients in the forcing at the

gridscale.

The basic formulas for the vertical volume flux via entrainment for a point source plume

(representing the discharge plume) and a sheet plume (representing the distributed melt

plume) that are used in these plume parameterizations (as well as the theory in Section 4)

can be derived from classic self-similarity and entrainment assumptions (see e.g., Morton,

Taylor, and Turner (1956)). To provide context for our theory, the following is a brief

overview of the fundamental aspects of plume theory.

An idealized axisymmetric turbulent plume can be defined in terms of parameters B

(buoyancy flux) and r (radial length scale), which are functions of z (height above the

source). For a constant background density, it is often assumed that plume profiles are

self-similar and dimensional analysis can be used to find the vertical velocity w, reduced

gravity g', and r as a function of z. Alternatively, for background density profiles that vary

with height, and the plume parameterization used in our model configuration, the vertical

properties of the plume are found numerically by solving a set of differential equations,

i.e., the conservation of mass, momentum, and buoyancy flux (based on Turner (1979)):

$$\frac{\partial m}{\partial z} = 2\alpha m/r \,, \tag{1a}$$

$$\frac{\partial mw}{\partial z} = mg'/w \,, \tag{1b}$$

$$\frac{\partial mg'}{\partial z} = -mN^2(z) \,, \tag{1c}$$

for a plume entrainment mass flux $m = r^2 w$. A similar set of equations can also be derived

for the front-wide melt plume by imposing a distributed buoyancy flux and can also be

solved numerically (see Turner (1979)). For a more complete plume formulation which

includes temperature, salinity, and density profiles that vary with depth (such as the one

implemented in our model), see Cowton et al. (2015).

In order to arrive at the simplifications to the overturning theory discussed in Section

4 (which are discharge- and melt plume-driven), we can approximate the solution to

Eqs. (1a)-(1c) by assuming an approximately uniform density below the depth of neutral

buoyancy (which is a fairly accurate approximation given the weak stratification below

the neutral buoyancy depth in many of Greenland's fjords; see e.g., Straneo and Cenedese

(2015)). This approximation allows the buoyancy flux equation (Eq. (1c)) to be simplified

to

$$B = mg' \,, \tag{2}$$

which results in the self-similar discharge plume solutions used in Section 4.1 (see Straneo and Cenedese (2015) for a discussion). The melt rate that is used for the buoyancy flux of the melt-driven plume can be approximated to be uniform with depth for simplicity (approximately a vertical mean) for the simplified overturning circulation approximation theory in Section 4.1, which allows for a similarity solution for the melt plume component used in Eq. (4) (in the main text).

S-2. Quasi-Streamfunction Discussion

We note that the quasi-streamfunction defined in Eq. (3) (in the main text) is only approximately equal to the 3D streamfunction, which can be defined via the relationship $(u, v, w) = \nabla \times \Psi_3$. The horizontal velocity field (u, v) is unlikely to be exactly nondivergent anywhere, but over most of the fjord, the horizontal velocity field is approximately nondivergent, i.e., the x- and y-components of the streamfunction vector are approximately zero and the flow is approximately described by the z-component of the streamfunction. The lack of boundary-incident streamlines in Fig. 2e in the main text and Fig. S4 suggests that the horizontal velocity field is indeed approximately nondivergent. Since the calculation of this quasi-streamfunction is calculated by taking the integral in the across-fjord direction, the interior quasi-streamfunction is largely unaffected by the eastern and western boundary nudged regions.

S-3. Fjord Circulation and Melt Sensitivity to Discharge Plume Strength, Geometry, Stratification, and Tides

This section provides additional exposition of the dependence of the fjord circulation and melt on the various model control parameters discussed in Section 3 of the main

text. Figs. S2-S6 shows the time-averaged meridionally-averaged temperature and salinity, overturning circulation, and vertically-integrated horizontal recirculation, and glacial melt rates for 9 endmember cases. All of the parameter variations seen here substantially influence the circulation and/or melt rate and suggest that these properties are all likely to be important when considering overturning, recirculation, and melt rates in real fjord systems.

The overturning circulation in the greatest discharge strength case $Q_0 = 1000$ m^3/s (Fig. S4d) increases by a factor of 2.5 compared to the $Q_0 = 100$ m^3/s case (Fig. S4c), but the overall melt rate only increases by 30% (Fig. S6c, d). Similarly to the reference case, the discharge plume and melt plume with a high discharge ($Q_0 = 1000$ m^3/s) is also additive, but the discharge-driven shallow overturning cell dominates the peak overturning strength (Fig. S4d). The increase in discharge primarily increases the magnitude of the shallow overturning circulation, which increases the shallow recirculation. An important takeaway is that at these depths, the recirculation (in Fig. S5d) has a much smaller impact on the overall melt rate.

Decreasing the sill height removes barriers of warm water access to the fjord (Fig. S2e) and increases melt rates by 20% for the case with no sill relative to the reference case (Fig. S6e). Increasing the fjord width from 6 km to 15 km approximately doubles the recirculation (Fig. S5f) and also doubles the melt rates (Fig. S6f) for the $W = 25$ km case. Decreasing the fjord depth weakens the overturning circulation (Fig. S4g) and melts a smaller cross-sectional glacial surface area, which results in a 25% decrease in melt rate for the shallow depth case ($H_\mathrm{fj} = 600$ m) compared to the reference case (Fig. S5g).

August 18, 2021, 12:20am

Increasing the surface stratification slightly strengthens the deep overturning (Fig. S4h), recirculation (Fig. S5h), and therefore, melt rate (Fig. S6h). The strength of the tides can also amplify the overturning circulation at the glacial face at depths near the sill maximum depth and can lead to a 30% increase in overall melt rates (Fig. S6i) for a barotropic tidal amplitude of 0.1 m/s.

S-4. Melt Rate Theory Approximations

The expressions and approximations used in Section 4.3 on the melt rate theory are a variation of the three-equation system of equations (Hellmer & Olbers, 1989; Holland & Jenkins, 1999) which describes the thermodynamical equilibrium at the ice-ocean interface. This equilibrium can be expressed using approximate heat and salt conservation and the linearized freezing temperature of seawater,

$$M(L_i + c_i(T_b - T_i)) = \gamma_T c_w(T_p - T_b) \tag{3a}$$

$$MS_b = \gamma_S(S_p - S_b), \tag{3b}$$

$$T_b = \lambda_1 S_b + \lambda_2 + \lambda_3 z, \tag{3c}$$

where $M, L_i, c_w, c_i, C_d, T_b, T_i, T_p$ are defined in Section 4.3, S_p is the plume salinity, S_b is the boundary layer salinity, γ_S is the turbulent salt transfer coefficient, and $\lambda_1 = -5.73 \times 10^{-2}$ °C psu^{-1}, $\lambda_2 = 8.32 \times 10^{-2}$ °C, and $\lambda_3 = 7.61 \times 10^{-4}$ °C m^{-1} are the freezing point slope, offset, and depth. These empirical values are consistent with those used in previous studies (Sciascia et al., 2013; Cowton et al., 2015). Recent parameterizations of the turbulent transfer coefficients (Jenkins et al., 2010) express the turbulent transfer coefficients in terms of near-glacial ocean velocities as

$$\gamma_T = C_d^{1/2} \Gamma_T \sqrt{v^2 + w^2}, \tag{4a}$$

$$\gamma_S = C_d^{1/2} \Gamma_S \sqrt{v^2 + w^2}, \tag{4b}$$

with C_d, Γ_T, v, w as defined in Section 4.3, and $\Gamma_S = 6.2 \times 10^{-4}$ is the salt transfer constant.

For simplicity, our theory in Section 4.3 for the melt rate M only uses Eqs. (3a) and (4a), since the plume and boundary layer temperature can be evaluated in our model directly (and does not vary significantly over the cases tested). We can then integrate the melt rate outside the discharge plume regions (which allows us to simplify $\sqrt{v^2 + w^2}$ to v) since this is where the majority of the melt occurs.

References

Cowton, T., Slater, D., Sole, A., Goldberg, D., & Nienow, P. (2015). Modeling the impact of glacial runoff on fjord circulation and submarine melt rate using a new subgrid-scale parameterization for glacial plumes. *J. Geophys. Res. Oceans*, *120*, 796–812.

Hellmer, H. H., & Olbers, D. J. (1989). A two-dimensional model for the thermohaline circulation under an ice shelf. *Antarctic Science*, *1*(4), 325–336. doi: 10.1017/ S0954102089000490

Holland, D. M., & Jenkins, A. (1999). Modeling Thermodynamic Ice-Ocean Interactions at the Base of an Ice Shelf. *J. Phys. Oceanogr.*, *29*(8), 1787–1800. doi: 10.1175/ 1520-0485(1999)029⟨1787:MTIOIA⟩2.0.CO;2

Jackett, D. R., & McDougall, T. (1995). Minimal adjustment of hydrographic profiles to achieve static stability. *J. Atmos. Ocean. Technol.*, *14*(4), 381–389.

Jenkins, A., Dutrieux, P., Jacobs, S., McPhail, S., Perrett, J., Webb, A., & White, D. (2010). Observations beneath Pine Island Glacier in West Antarctica and implica-

tions for its retreat. *Nat. Geosci.*, *3*, 468–472.

Morton, B. R., Taylor, G. I., & Turner, J. S. (1956). Turbulent gravitational convection from maintained and instantaneous sources. *Proceedings of the Royal Society of London. Series A. Mathematical and Physical Sciences*, *234* (1196), 1-23. doi: 10 .1098/rspa.1956.0011

Sciascia, R., Straneo, F., Cenedese, C., & Heimbach, P. (2013). Seasonal variability of submarine melt rate and circulation in an East Greenland fjord. *J. Geophys. Res. Oceans*, *118*, 2492–2506.

Straneo, F., & Cenedese, C. (2015). The Dynamics of Greenland's Glacial Fjords and Their Role in Climate. *Annu. Rev. Mar. Sci.*, *7*(1), 89-112. doi: 10.1146/annurev -marine-010213-135133

Turner, J. S. (1979). *Buoyancy effects in fluids. Cambridge University Press Paperback.*

Zhao, K. X., Stewart, A. L., & McWilliams, J. C. (2021). Geometric Constraints on Glacial Fjord–Shelf Exchange. *J. Phys. Oceanogr.*, *51 (4)*, 1223–1246. doi: 10.1175/ JPO-D-20-0091.1

Name	Parameter	Test Cases	Test Name	Units
Sill Height	H_S	$[0, \mathbf{150}, 200, 250]$	$[S_0, - , S_{150}, S_{200}, S_{250}]$	m
Fjord Width	W_{fj}	$[4,\mathbf{6},9,15]$	$[W_4, - , W_9, W_{15}]$	km
Fjord Depth	H_{fj}	$[600, \mathbf{800}, 1000]$	$[D_{600}, - , D_{1000}]$	m
Fjord Length (constant)	L_{fj}	25		km
Subglacial Discharge	Q_0	$[0, \mathbf{100}, 300, 1000]$	$[Q_0, Q_{100}, Q_{300}, Q_{1000}]$	m^3/s
Melt Parameterization		[No melt, Boundary Layer Melt, **Melt Plume**]	$[- , M_{BL}, M_P]$	
Stratification	$\rho_3 - \rho_2$	$[0.25, \mathbf{0.45}, 0.65]$	$[\Delta\rho_{0.25} , - , \Delta\rho_{0.65}]$	kg/m^3
Tidal Amplitude	u_{tide}	$[\mathbf{0}, 0.05, 0.1]$	$[- , T_{0.05}, T_{0.1}]$	m/s

TABLE 1. Summary of key fjord parameters and test cases for the numerical simulations. All variables are independently varied relative to the reference case (in bold text).
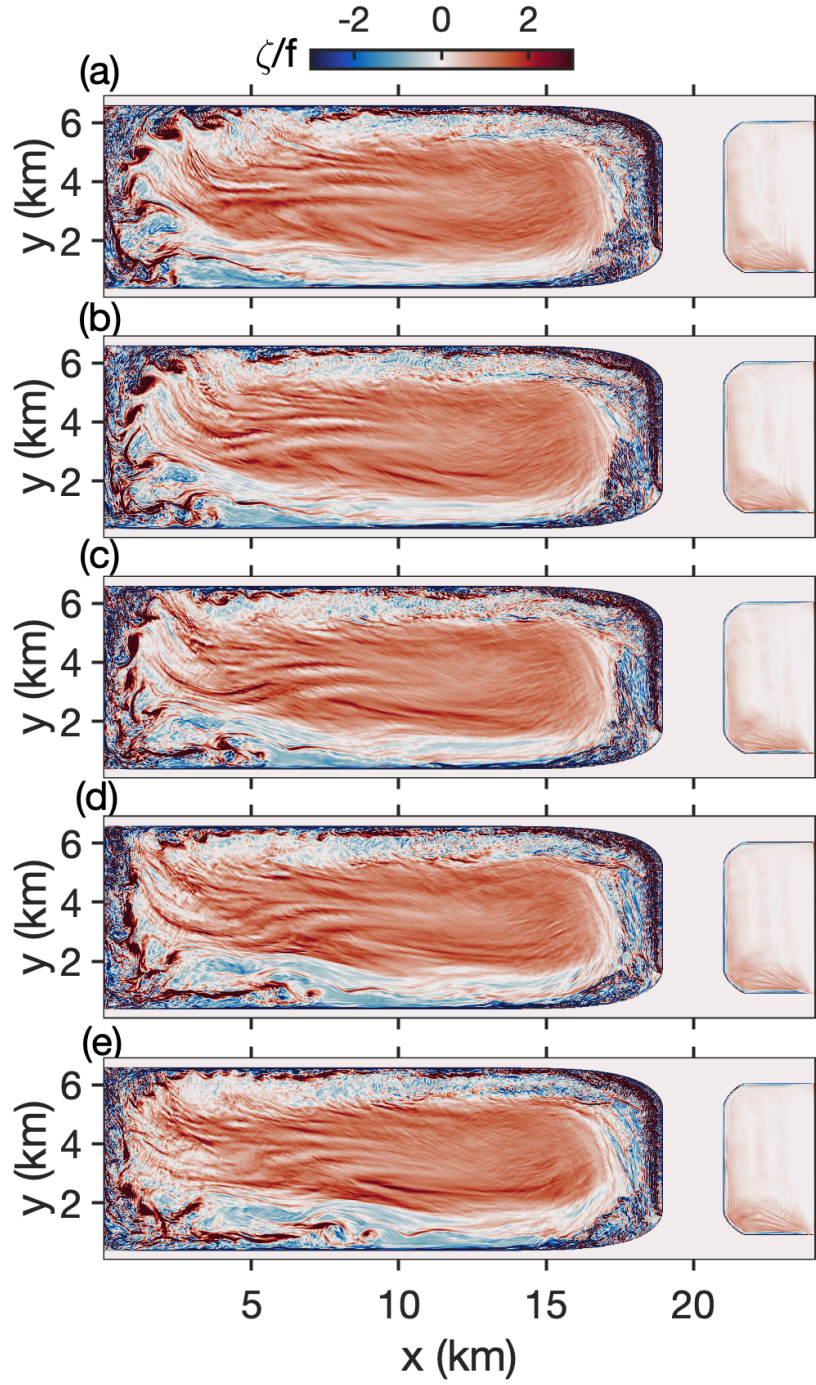
:

Figure S1. Snapshots of normalized vorticity of the reference simulation at $z = -320$ m at time (a) 90.0, (b) 90.1, (c) 90.2, (d) 90.3, (e) 90.4 days, showing a sequence of eddies being shed into the interior horizontal recirculation.
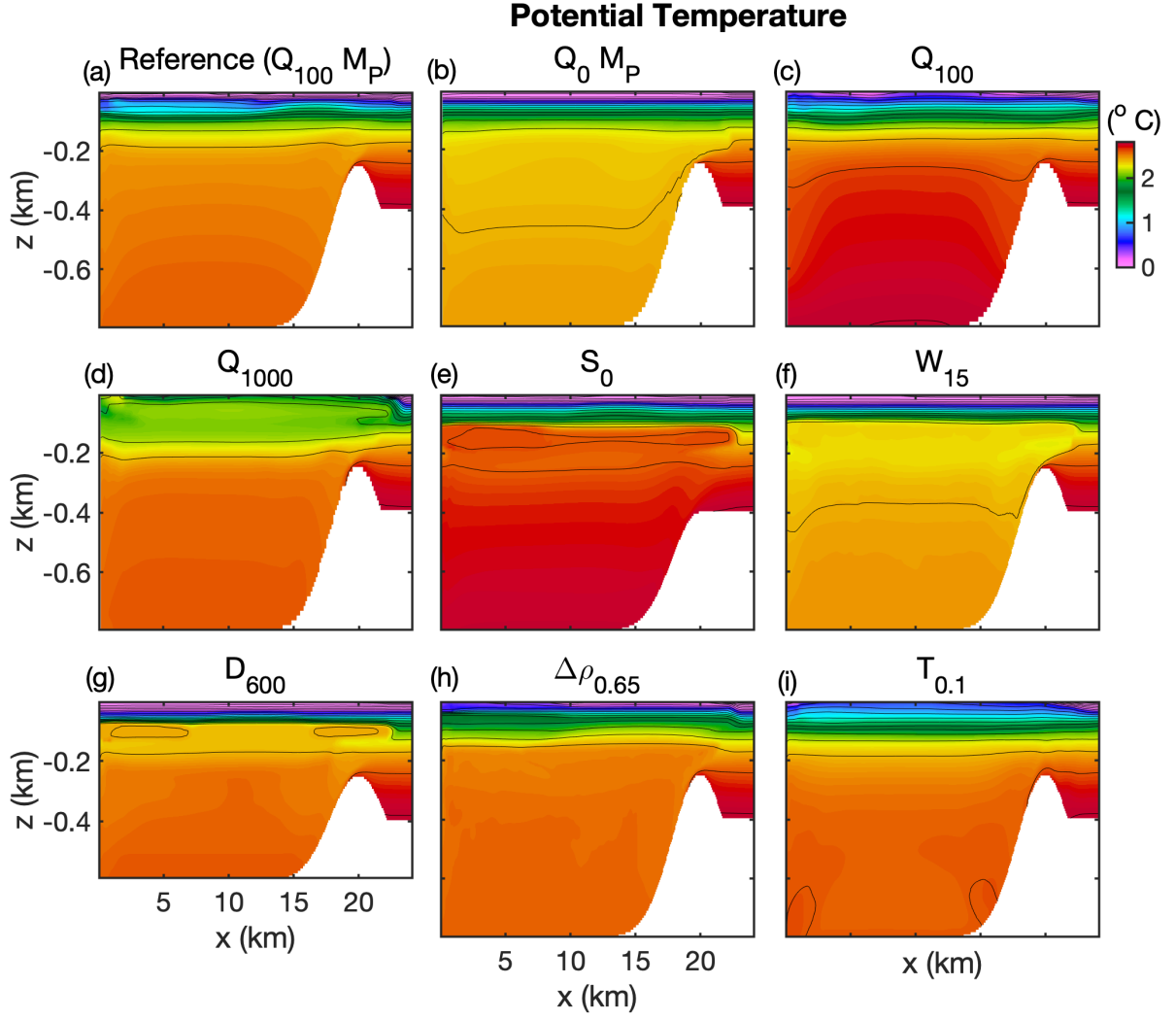
August 18, 2021, 12:20am

Figure S2. (a)-(i) Time- and meridionally-averaged potential temperature profiles for 9 experiments with varying parameters (see Table S1 for specific parameters for each case). The contour spacing is $0.2\,^{\circ}\mathrm{C}$.
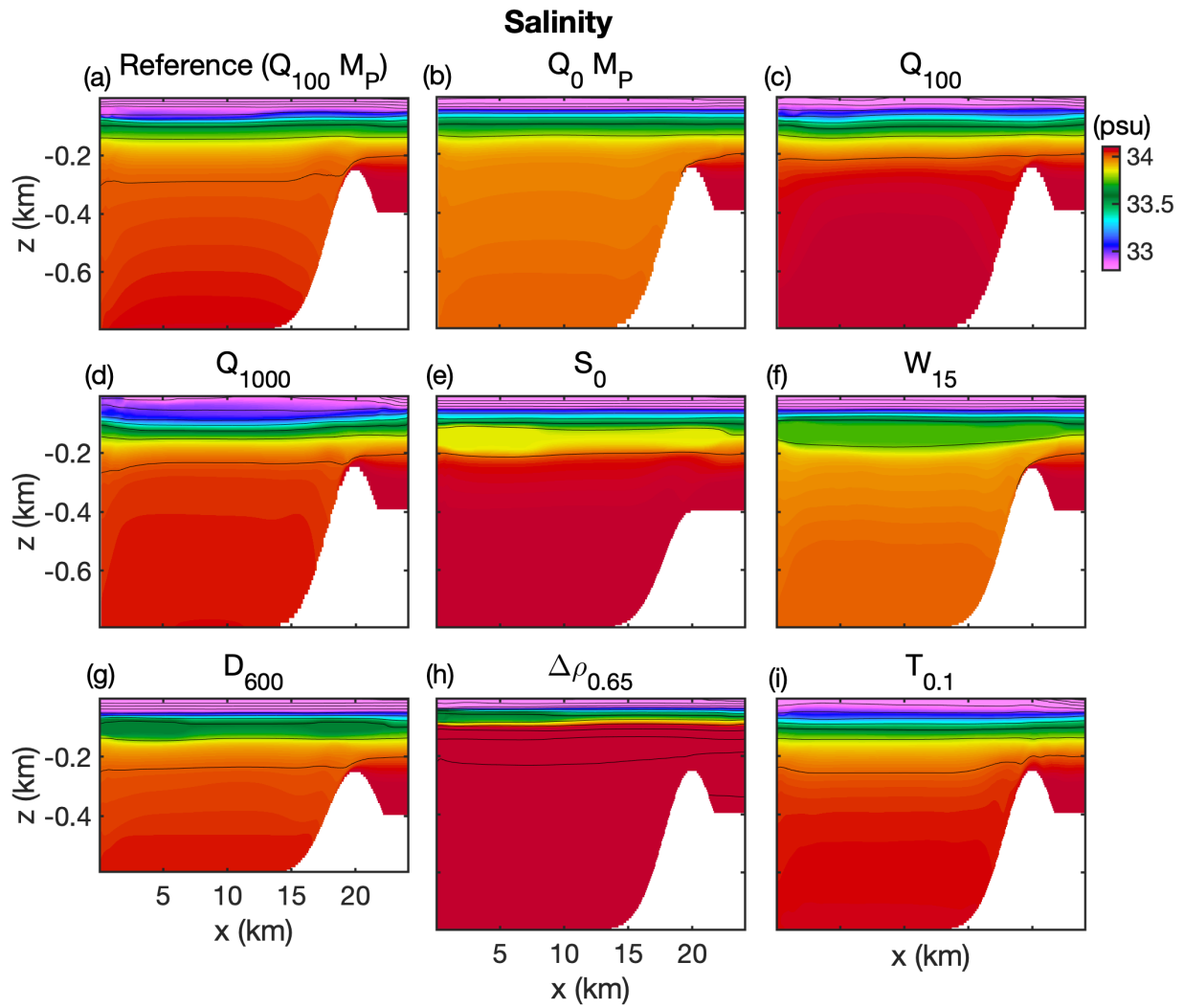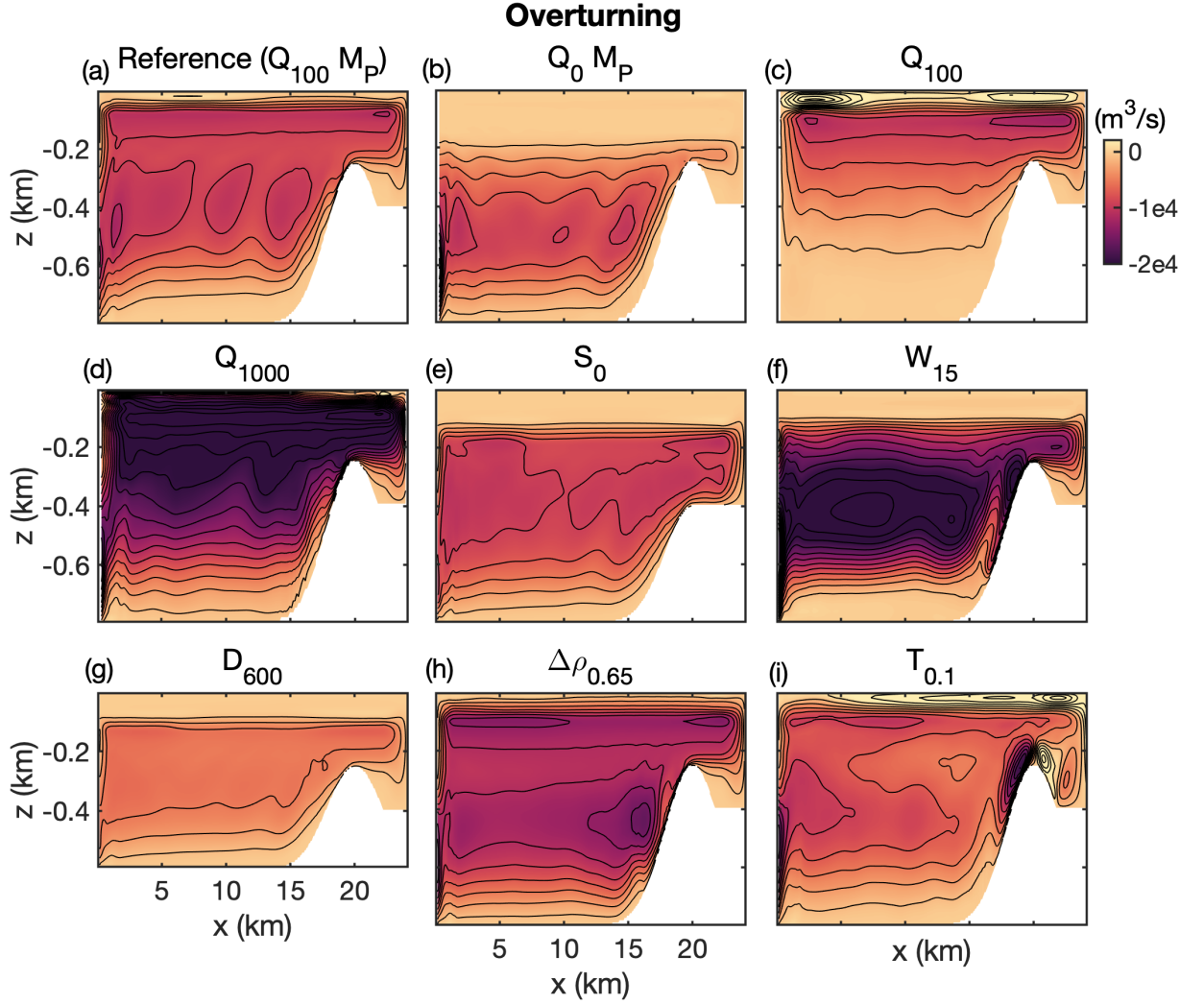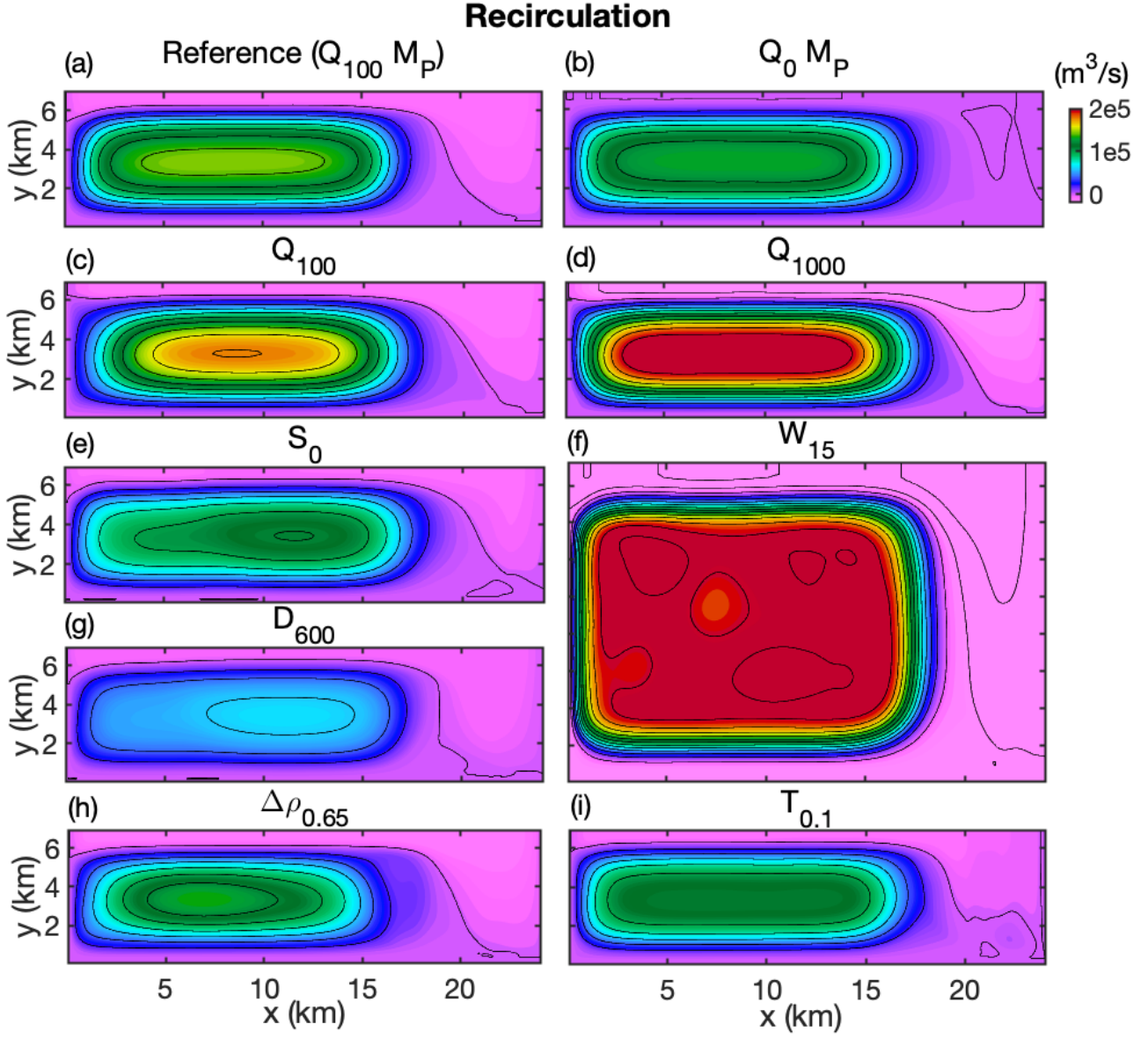
August 18, 2021, 12:20am

Figure S3. (a)-(i) Time- and meridionally-averaged salinity profiles for 9 experiments with varying parameters (see Table S1 for specific parameters for each case). The contour spacing is 0.2 psu.

Figure S4. (a)-(i) Time-averaged overturning circulation for 9 experiments with varying parameters (see Table S1 for specific parameters for each case). The contour spacing is 2×10^3 m^3/s.
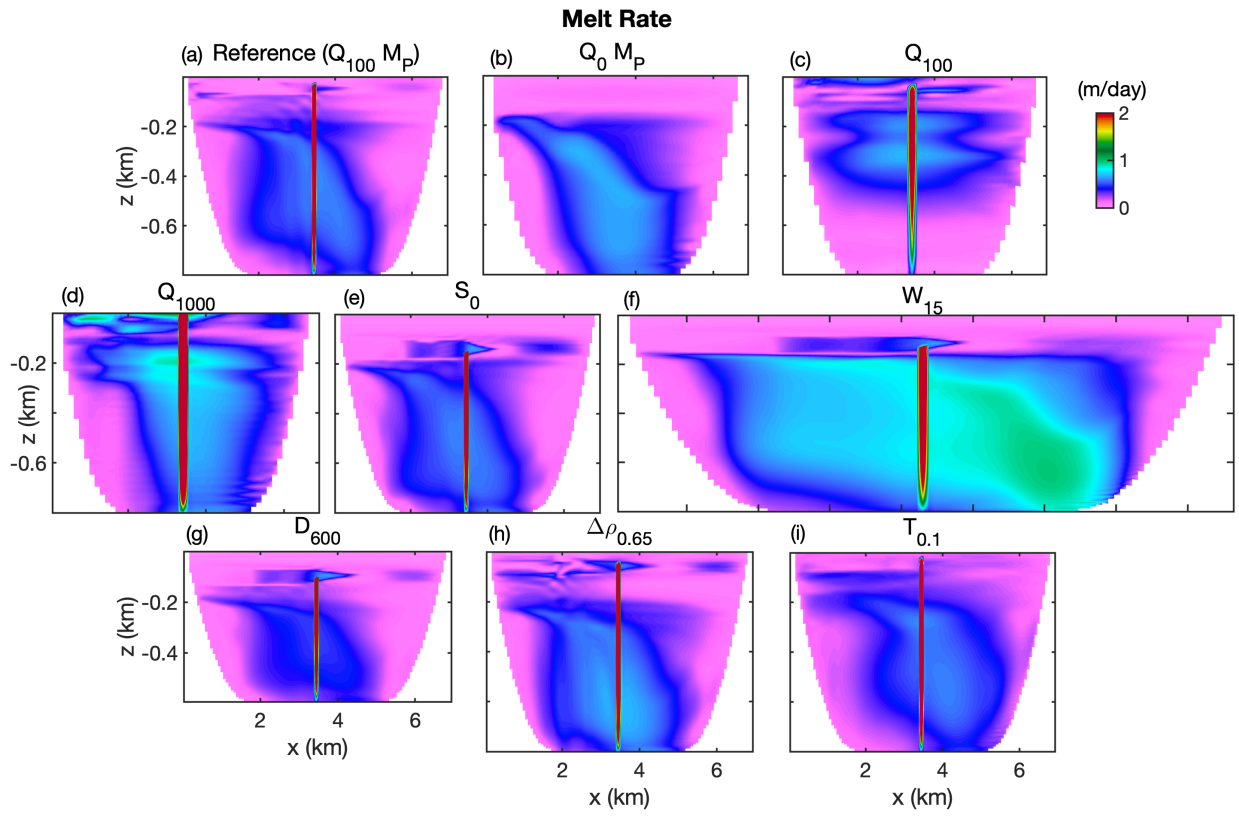
:

Recirculation

Figure S5. (a)-(i) Time-averaged horizontal recirculation integrated over depth (excluding circulation above the neutral buoyancy depth) for 9 experiments with varying parameters (see Table S1 for specific parameters for each case). The contour spacing is 2×10^4 m^3/s.

Melt Rate

Figure S6. (a)-(i) Time-averaged melt rates (m/day) at the glacial face for 9 experiments with varying parameters (see Table S1 for specific parameters for each case).
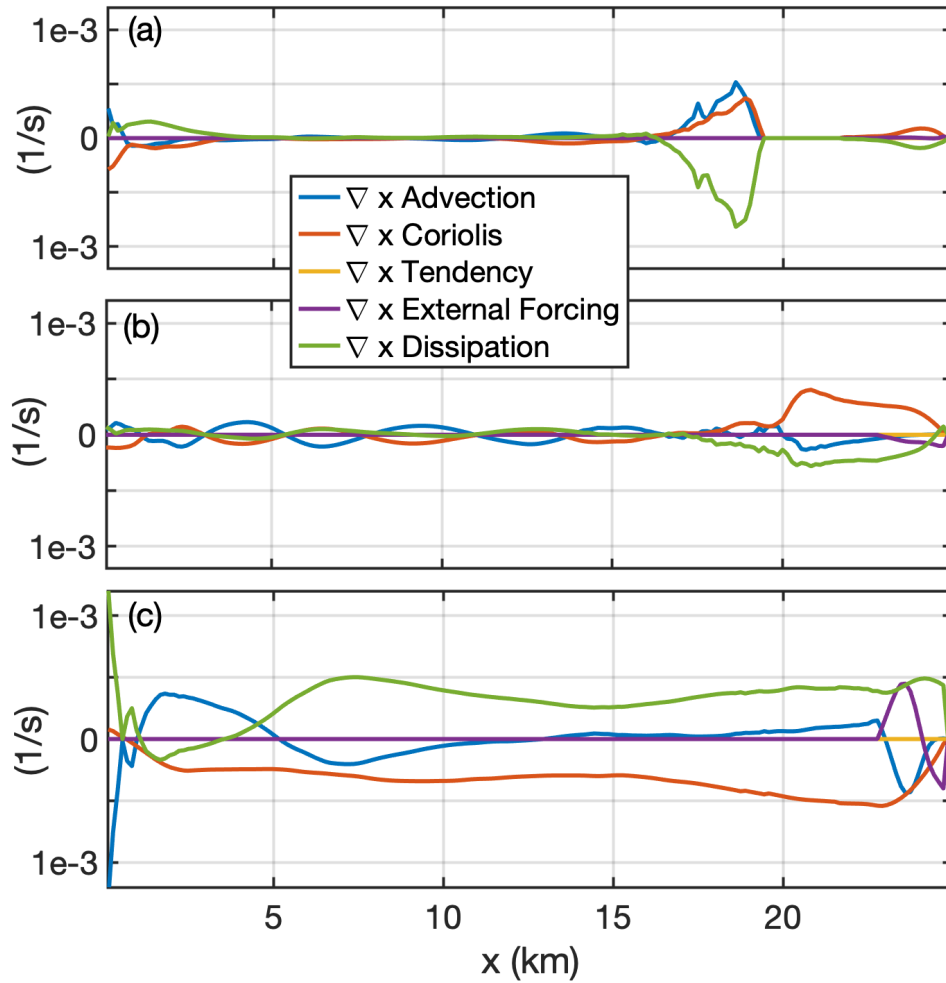
Figure S7. Vorticity balance in our reference experiment showing the depth-integrated meridionally-integrated curl of the momentum equation terms, cumulatively-integrated w.r.t. x starting from $x = 0$ in (a) the top 200 m, (b) -400 m $< z < -200$ m, and (c) the bottom 400 m. See Zhao et al. (2021) for a derivation of the terms used in the vorticity balance.
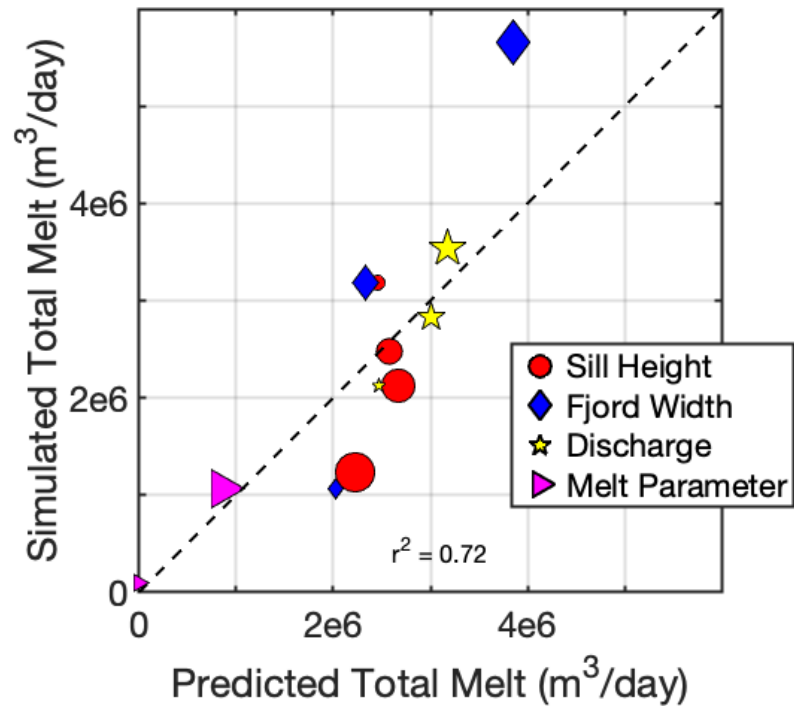
Figure S8. Simulation-diagnosed vs. theoretical predictions for the overall glacial melt rate based on the overturning and recirculation theory (Eqs. (11) and (10)).